Mathematical modeling for meshwork formation of endothelial cells in fibrin gels

佐々木, 大貴

Journal of Theoretical Biology 429 (2017) 95–104

Contents lists available at ScienceDirect

Journal of Theoretical Biology

journal homepage: www.elsevier.com/locate/jtbi

Mathematical modeling for meshwork formation of endothelial cells *in fibrin gels*

Daiki Sasaki[a,*], Hitomi Nakajima[b], Yoshimi Yamaguchi[a], Ryuji Yokokawa[c], Shin-Ichiro Ei[d], Takashi Miura[a]

[a] Department of Anatomy and Cell Biology, Kyushu University Graduate School of Medicine, Fukuoka, Japan
[b] Department of Biomedical Science,Kyushu University Faculty of Medicine, Fukuoka, Japan
[c] Department of Micro Engineering, Kyoto University, Kyoto, Japan
[d] Department of Mathematics, Hokkaido University, Hokkaido, Japan

ARTICLE INFO

Article history:
Received 14 January 2017
Revised 20 May 2017
Accepted 10 June 2017
Available online 23 June 2017

Keywords:
Vasculogenesis
HUVEC
Pattern formation
Cytoskeleton
Delay differential equation

ABSTRACT

Vasculogenesis is the earliest process in development for spontaneous formation of a primitive capillary network from endothelial progenitor cells. When human umbilical vein endothelial cells (HUVECs) are cultured on Matrigel, they spontaneously form a network structure which is widely used as an in vitro model of vasculogenesis. Previous studies indicated that chemotaxis or gel deformation was involved in spontaneous pattern formation. In our study, we analyzed the mechanism of vascular pattern formation using a different system, meshwork formation by HUVECs embedded in fibrin gels. Unlike the others, this experimental system resulted in a perfusable endothelial network in vitro. We quantitatively observed the dynamics of endothelial cell protrusion and developed a mathematical model for one-dimensional dynamics. We then extended the one-dimensional model to two-dimensions. The model showed that random searching by endothelial cells was sufficient to generate the observed network structure in fibrin gels.

1. Introduction

The circulatory system is the first organ system to function during development (Drake, 2003; Gilbert, 2014). Initially, aggregations of hemangioblasts, called blood islands, appear and connect with one another to form a primitive vascular plexus. This process is called *vasculogenesis*. After establishment of these primitive blood vessels, additional new blood vessels are generated by sprouting from preexisting vessels. This process is called *angiogenesis* (Adams and Alitalo, 2007).

In previous studies, human umbilical vein endothelial cells (HUVECs) cultivated on Matrigel (Matrigel system) were used as an experimental system of vasculogenesis. It is well known that some endothelial cells form a meshwork resembling a capillary plexus on Matrigel (Kubota et al., 1988; Miura and Tanaka, 2009). Several mathematical models of this system were proposed. One class of models used a deformation of the extracellular matrix (Manoussaki et al., 1996; van Oers et al., 2014). Another type of models used chemotaxis toward vascular endothelial growth factor (VEGF) (Serini et al., 2003) (Fig. 1).

Methods to create artificial vascular plexuses have been extensively studied in the field of bioengineering (Miura and Yokokawa, 2016). These methods may be classified into two categories: predesigned method and self-organizing method (Hasan et al., 2014). As an example of the latter, we utilized meshwork formation by HUVECs embedded in fibrin gels (fibrin gel system) (Kim et al., 2013). This system is functionally better than the Matrigel system because it spontaneously develops a *perfusable* capillary meshwork without any artificial scaffolds or patterns. However, the mechanism of meshwork formation in this system has not been elucidated.

In our study, we monitored the time course of pattern formation in fibrin gel by confocal microscopy, finding that the pattern formation mechanism in fibrin gel was very different from that on Matrigel. Meshwork formation by random endothelial protrusion at the early phase of culture determined the network pattern ultimately formed in this system. Based on our observations, we formulated a one-dimensional (1D) model of the extension/collapse dynamics of the cell protrusions. We analytically derived the connection probability between cells in this system. We then developed a two-dimensional (2D) model by incorporating cell size and distribution. Numerical simulation of the model reproduced the experimentally observed meshwork morphology. We assayed two

* Corresponding author.

http://dx.doi.org/10.1016/j.jtbi.2017.06.012
0022-5193/

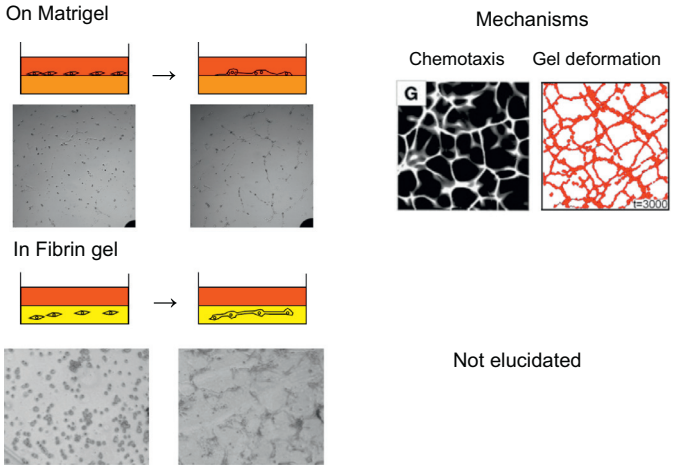

Fig. 1. Mechanisms of in vitro vasculogenesis. When endothelial cells are cultivated on Matrigel or in a fibrin gel, they form network-like structures. Proposed mechanisms of pattern formation on Matrigel were chemotaxis toward VEGF (Serini et al., 2003) and mechanical gel deformation (Manoussaki et al., 1996; van Oers et al., 2014). Pattern formation mechanisms in fibrin gels, however, were not previously examined. Panels showing Matrigel model simulations were reprinted from van Oers et al. (2014); Serini et al. (2003).

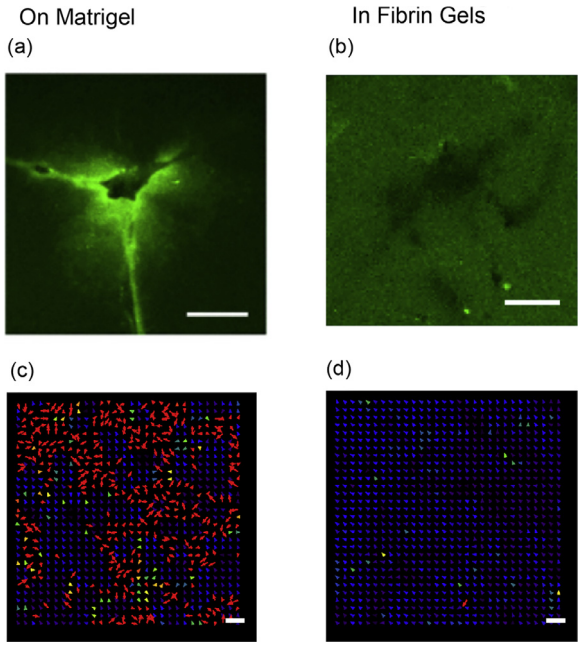

Fig. 2. Endothelial pattern formation inside the microdevice did not have the characteristics observed in the Matrigel system. (a) On Matrigel, VEGF was accumulated around HUVECs (reprinted from Köhn-Luque et al. (2013)). (b) In fibrin gels, VEGF accumulation around cells was not observed. (c) On Matrigel, each cell exerted strong traction forces. Small fluorescent particles were mixed with Matrigel and time-lapse images were obtained. Then gel movements were analyzed using particle image velocitometry (PIV). (d) In fibrin gels, cell traction of the extracellular matrix was not evident. Scale bars = 50 μm.

functional characteristics of the network, percolation and island size distribution. Our model should be useful for controlling network structures in vitro.

2. Experimental observation: endothelial meshwork formation during vasculogenesis *in fibrin gels*

2.1. The mechanism of meshwork formation in fibrin gels was different from that on Matrigel.

In mathematical studies of the Matrigel system, two mechanisms of meshwork formation were proposed, chemotaxis toward VEGF and gel deformation. These phenomena were confirmed experimentally (Fig. 2a, c). However, in fibrin gels, there was no VEGF gradient observed around cells (Fig. 2b) and no detectable deformation of the extracellular matrix (Fig. 2d). Detailed experimental procedures for the VEGF gradient visualization were described in Köhn-Luque et al. (2013). The difference in gel traction was statistically significant (See Appendix B and Supplemental video 1). In addition, cell movements were different in the Matrigel and fibrin gel systems. In the Matrigel system, cells moved collectively to form initial aggregates. In contrast, cells barely moved in fibrin gels. Therefore, the mechanism of endothelial meshwork formation in fibrin gels was different from that on Matrigel.

2.2. Observation of meshwork formation

We observed capillary formation and found that the initial meshwork pattern within 24 h determined that of the perfusable capillary network formed after a week (Fig. 3a). From this observation, we focused on cellular connections made by protrusions to elucidate the mechanism of generating the initial meshwork pattern.

We observed that connections by cellular protrusions enabled meshwork formation without cell movement. Time-lapse observations of fibrin gel cultures revealed that:

1. Cells did not move, but actively formed protrusions (Fig. 3b).
2. Protrusions underwent repeated cycles of extension and collapse (Fig. 3c).
3. When a protrusion collided with the surface of an adjacent cell, a connection was usually established (23/20) (Fig. 3d).
4. Collisions between protrusions (8/21) were fewer than collisions between a protrusion and cell body (13/21).
5. Formation of the protrusion was not affected by neighboring cells (Fig. 3e, f).
6. Speed of collapse was greater than that of extension (Fig. 3g, h).
7. Two neighboring cells had a higher probability of connecting when they were closer to one another.

3. Model definition

3.1. Discrete-time stochastic model for protrusion dynamics

We formulated a model for protrusion dynamics using a discrete-time stochastic process. A protrusion whose initial length is 0 extends at a rate c (It was assumed to be a positive integer for simplicity.) per unit time and it connects to a neighboring cell when it collides with the surface of that cell. The protrusion collapses at probability $p(>0)$ per unit time and the length then instantaneously becomes 0. Assuming the length of a protrusion at time τ is A_τ, this process is expressed as follows:

$$\begin{cases} Pr(A_{\tau+1} = A_\tau + c) = 1 - p \\ Pr(A_{\tau+1} = 0) = p. \end{cases} \quad (1)$$

The transition diagram of the process is expressed in Fig. 4a. We can describe the model by a transition matrix as follows:

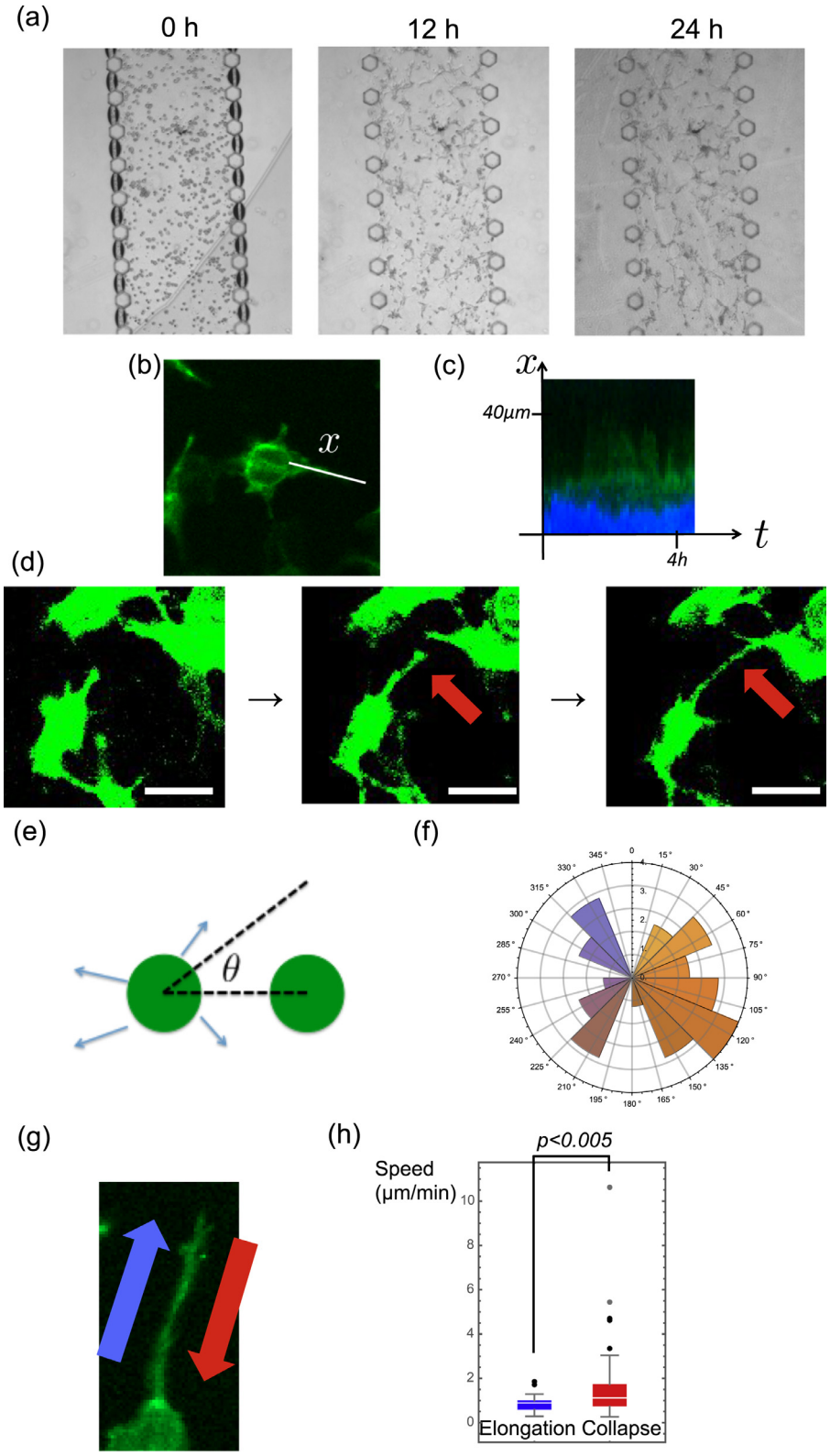

Fig. 3. Observation of protrusion dynamics and meshwork formation. (a) Observation of meshwork formation in fibrin gels for 24 h. HUVECs mixed with fibrin gels were injected into a microchannel separated by hexagonal pillars. Cells extended protrusions and formed networks within 24 h. (b) Observation of protrusions. HUVECs were stained with UEA1-Alexa 488 (green) and embedded in fibrin gels and their movements were observed for 12 h. HUVECs extended many thin protrusions, with lengths of up to 100 μm. (c) Kymograph of a protrusion. Protrusions showed frequent extensions and collapses, while nuclei seldom moved. Nuclei were stained with Hoechst 33342 (bottom of the picture). (d) Establishment of a connection by collision of a protrusion with a cell body (red arrows). Scale bars = 50 μm. (e) Effects of an adjacent cell on protrusion formation. We defined the angle between the line connecting the centers of cells and the protrusion as θ. (f) Rose diagram of protrusion formation. We used maximum intensity projection of 8 cells, 29 protrusions. Degrees around the circle are θ and radii of sectors are frequency. Formation of protrusions was not affected by adjacent cells. (g) Differences in speed of extension and collapse. (h) Collapse speed ($\simeq$ 1.75 μm/min) was higher than extension speed ($\simeq$ 0.86 μm/min). The difference was statistically significant ($p < 0.005$, Mann-Whitney U test). Even with the outlier removed, the difference remained statistically significant. (For interpretation of the references to colour in this figure legend, the reader is referred to the web version of this article.)

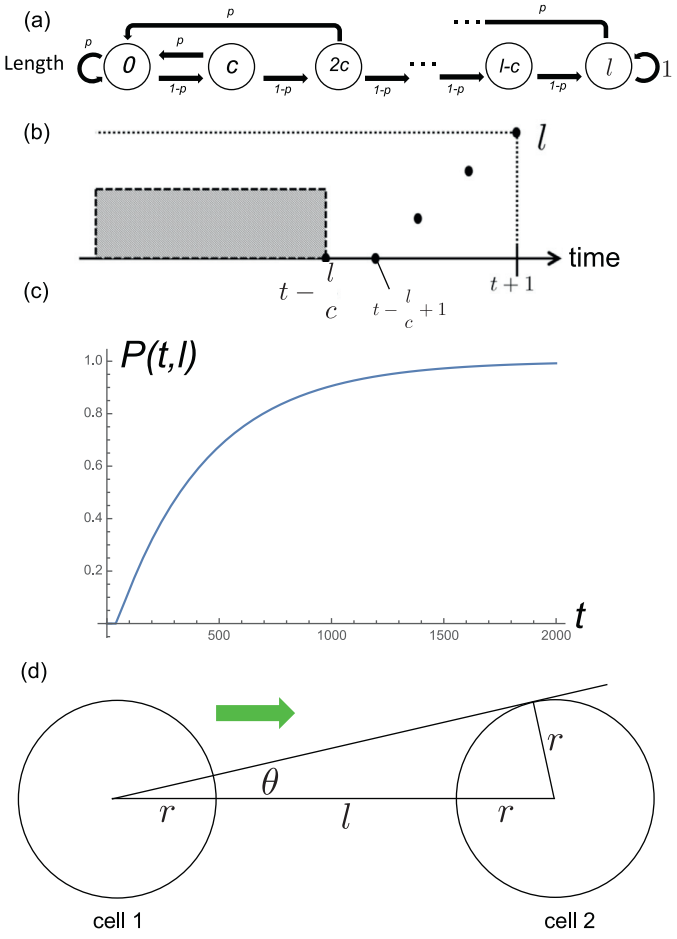

Fig. 4. Definition of the stochastic model. (a) Transition probability of length. (b) Intuitive explanation of the last term of the recurrence equation. The condition "to connect at time $(t+1)$ for the first time" must satisfy three requirements: 1. The protrusion does not collide from time 1 to time $(t-l/c)$. 2. Collapse occurs at time $(t-l/c+1)$. 3. A protrusion of length l is established at time $(t+1)$. (c) A graph of $P(t, l)$ function. It shows an increasing function for time and $P(t, l) \to 1$ for $t \to \infty$. Parameters are $l = 50$, $p = 0.0562$ and $c = 0.86$. (d) Two cells are present in a two-dimensional field. Assuming that cells are circles, protrusions extend straight and each cell has an average number of a protrusions, we consider the situation that a protrusion from cell 1 collides with cell 2.

$$\begin{pmatrix} Pr(A_{\tau+1}=0) \\ Pr(A_{\tau+1}=c) \\ Pr(A_{\tau+1}=2c) \\ \vdots \\ Pr(A_{\tau+1}=l-c) \\ Pr(A_{\tau+1}=l) \end{pmatrix} = \begin{pmatrix} p & p & p & \dots & p & 0 \\ 1-p & 0 & 0 & \dots & 0 & 0 \\ 0 & 1-p & 0 & \dots & 0 & 0 \\ \vdots & \ddots & \ddots & \ddots & \ddots & \vdots \\ 0 & 0 & 0 & \dots & 0 & 0 \\ 0 & 0 & 0 & \dots & 1-p & 1 \end{pmatrix} \times \begin{pmatrix} Pr(A_{\tau}=0) \\ Pr(A_{\tau}=c) \\ Pr(A_{\tau}=2c) \\ \vdots \\ Pr(A_{\tau}=l-c) \\ Pr(A_{\tau}=l) \end{pmatrix}. \quad (2)$$

We also assumed a time for meshwork formation as t, the distance between the neighboring cells as l and a connection probability function as $P(t, l)$. When $\frac{l}{c}$ is an integer, the following recurrence relation holds:

$$\begin{aligned} P(t+1,l) &= Pr(A_{t+1}=l) \\ &= Pr(A_t=l) + Pr(A_t=l-c)(1-p) \\ &= Pr(A_t=l) + Pr(A_{t-1}=l-2c)(1-p)^2 \\ &= \dots \\ &= Pr(A_t=l) + Pr(A_{t-\frac{l}{c}+1}=0)(1-p)^{\frac{l}{c}} \\ &= Pr(A_t=l) + p\sum_{i=-\infty}^{\frac{l}{c}-1} Pr(A_{t-\frac{l}{c}}=ci)(1-p)^{\frac{l}{c}} \\ &= Pr(A_t=l) + p\{1-Pr(A_{t-\frac{l}{c}}=l)\}(1-p)^{\frac{l}{c}} \\ &= P(t,l) + p\{1-P(t-\frac{l}{c},l)\}(1-p)^{\frac{l}{c}}. \end{aligned} \quad (3)$$

For all positive integers t and l, $P(t, l)$ can be evaluated from this recurrence relation and the boundary conditions

$$\begin{cases} P(t,l)=0 & (t < l/c) \\ P(t,l)=(1-p)^{\frac{l}{c}} & (t=l/c). \end{cases} \quad (4)$$

The boundary conditions are obtained as follows: (i) When $t < l/c$, the length of a protrusion is smaller than l because the highest possible length is $ct(<l)$. Therefore $P(t, l) = 0$. (ii) When $t = l/c$, a connection is established only if the protrusion has been extending continuously during previous intervals of time. The connection probability is equal to the probability of the protrusion continuing to extend (See also Fig. 4b).

3.2. Continuum limit of the recurrence relation

The continuum limit of the recurrence relation is obtained by extending to real t and l greater or equal to 0. Replacing the time step by Δt, (3) is expressed as follows:

$$\begin{aligned} P(t+\Delta t,l) &= P(t,l) + Pr(A_t=l-c\Delta t)(1-p\Delta t) \\ &= P(t,l) + Pr(A_{t-\Delta t}=l-2c\Delta t)(1-p\Delta t)^2 \\ &= \dots \\ &= P(t,l) + Pr(A_{t-\frac{l}{c}+\Delta t}=0)(1-p\Delta t)^{\frac{l}{c\Delta t}} \\ &= P(t,l) + \{1-P(t-\frac{l}{c},l)\}p\Delta t(1-p\Delta t)^{\frac{l}{c\Delta t}}. \end{aligned} \quad (5)$$

Taking the limit of $\Delta t \to 0$, we obtain a differential equation with boundary conditions,

$$\begin{cases} \frac{dP}{dt} = pe^{-\frac{lp}{c}}\{1-P(t-\frac{l}{c},l)\} \\ P(t,l)=0 \quad (t<\frac{l}{c}) \\ P(\frac{l}{c},l)=e^{-\frac{lp}{c}}. \end{cases} \quad (6)$$

We can obtain the same equation from the probability density function of protrusion length (See Appendix C).

3.3. Analytical solution

Now an analytical solution of the Eq. (6) can be obtained. Although (6) is a delay differential equation, it is solved as follows, using periodicity:

$$P(t,l) = \begin{cases} \sum_{k=1}^{[\frac{ct}{l}]}\{\frac{(-p)^{k-1}}{k!c^k}e^{-\frac{lp}{c}k}(ct-kl)^{k-1}(kc-klp+cpt)\} & (ct \geq l) \\ 0 & (ct < l) \end{cases} \quad (7)$$

where $[\frac{ct}{l}]$ shows the largest integer which does not exceed $\frac{ct}{l}$. The detailed derivation is described in Appendix D.

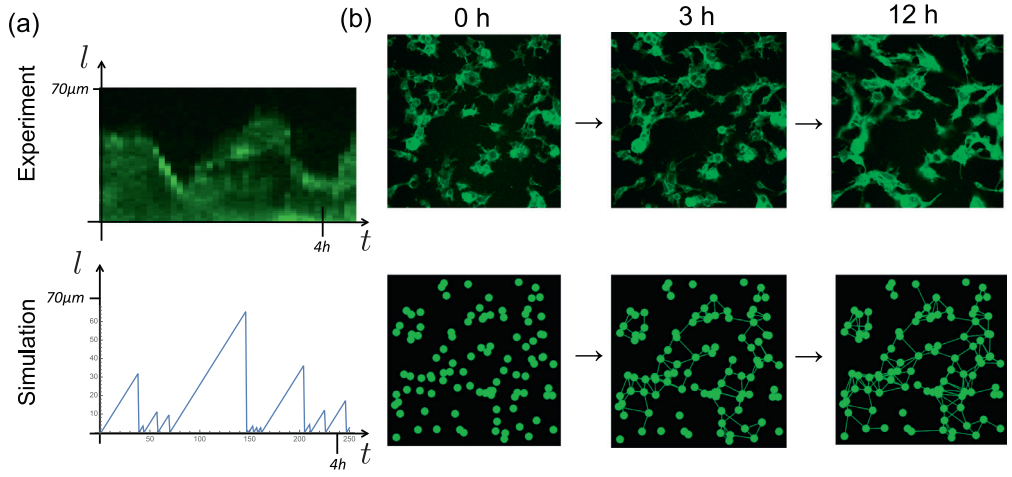

Fig. 5. Results of numerical simulations. (a) Kymographs obtained from experimental data and from a numerical simulation of the model. Model dynamics reproduced the experimental observations. (b) Meshwork morphology obtained from observation and numerical simulation.

3.4. Derivation of connection probability for two cells in two dimensions

Now we consider cell-cell connections by protrusion. Using $P(t, l)$, we obtained the connection probability of two cells, cells 1 and 2, in a two-dimensional field, $P_{cell}(t, l)$. We assume that cells are circles of radius r and that protrusions extend straight in a circumferential direction (Fig. 4d). We define an average number of protrusions per cell as a. The probability that one protrusion extends in a connectable direction is $\frac{2\theta}{2\pi} \simeq \frac{\sin\theta}{\pi} = \frac{r}{\pi(2r+l)}$ and the probability that a protrusion from cell 1 collides with cell 2 can be approximated as $P(t, l)$. $P_{cell}(t, l)$ is the complement of the event in which none of a protrusions establishes a connection. Therefore $P_{cell}(t, l)$ is expressed as follows:

$$P_{cell}(t, l) \simeq 1 - \{1 - \frac{r}{\pi(2r+l)} P(t, l)\}^a. \quad (8)$$

4. Numerical experiment

4.1. Model implementation

Numerical simulations were performed using *Mathematica*. Source codes are provided in supplemental material.

4.2. The discrete-time stochastic model reproduced protrusive dynamics

Fig. 5a shows kymographs obtained from experimental data and from a numerical simulation of the model. Model dynamics and experimental observations were similar in that protrusion extended and collapsed and collapse speed was greater than extension speed. See also supplemental video 2.

4.3. Simulation of meshwork formation

Before simulating meshwork formation, we obtained unknown parameters by length-connection probability relationships derived from experimental observations. In this experiment, $t = 12 \times 60(\text{min})$, $c = 0.86(\mu\text{m/min})$ and $r \simeq 15(\mu\text{m})$. By the least squares method, we derived values of unknown parameters as $a = 6.784$ and $p = 0.0562$ (Appendix E). Using t, c, r, a and p, we obtained a connection probability as a function of distance l. To reduce the amount of calculations, we regarded $P_{cell}(t, l)|_{l < 10}$ as $P_{cell}(t, 10)$. Cell number per focal plane was assumed to be 100. We neglected connections between protrusions because they are not responsible for meshwork morphology and crossing between protrusions can express clustering of cells. Numerical simulation reproduced the morphology of the observed endothelial meshworks (Fig. 5b). We also reproduced the time course of meshwork formation (Fig. 5b and Supplemental video 3, with the detailed mechanism described in Appendix F). In both experimental observations and numerical simulations, neighboring cells were connected to one another to form clusters within first 3 h, followed by meshwork formation by inter-cluster connections. In the 0 h image from experimental observations, several connections were already established because cells started extending protrusions during fibrin gel solidification and lectin staining.

4.4. Size distribution of islands in the simulation and the experiment

To assess the similarity of patterns in the numerical simulation and the experiment, we examined size distribution of the islands (Fig. 6). Analysis was performed using snapshots after 12 h. We ignored islands with sizes of less than 100 μm^2 because small islands represented noise in the experimental data and minute divisions by clusters of cells in the simulation results. The two histograms were similar and both distributions showed linearity in log-log plots, indicating that both sets of data obeyed certain power laws. Scaling exponents were −0.949 for experimental and −0.950 for simulation data (blue line in Fig. 6b).

4.5. Effects of simulation parameters on percolation

Whether the network is functional depends on whether it percolates. We defined the top five cells as the top end and bottom five cells as the bottom end. Meshworks were considered to percolate when connections existed between top and bottom ends. Simulations were performed 100 times for each parameter set. The same parameter set ($t = 12 \times 60(\text{min})$, $c = 0.86(\mu\text{m/min})$, $r \simeq 15(\mu\text{m})$, $a = 6.784$, $p = 0.0562$) was used, other than the parameter of interest.

Some percolation threshold appeared to exist in this system. The original parameter set was close to the percolation threshold (dashed line of Fig. 7), indicating that only a minor change in these parameters could result in loss of percolation.

We also compared critical density for percolation with a previous report on a Matrigel system (Gamba et al., 2003). A total of 94 cells/mm^2 in a Matrigel system and 251 cells/mm^2 in a fibrin gel system were required for percolation. This reflected the immobility of cell bodies in fibrin gels systems.

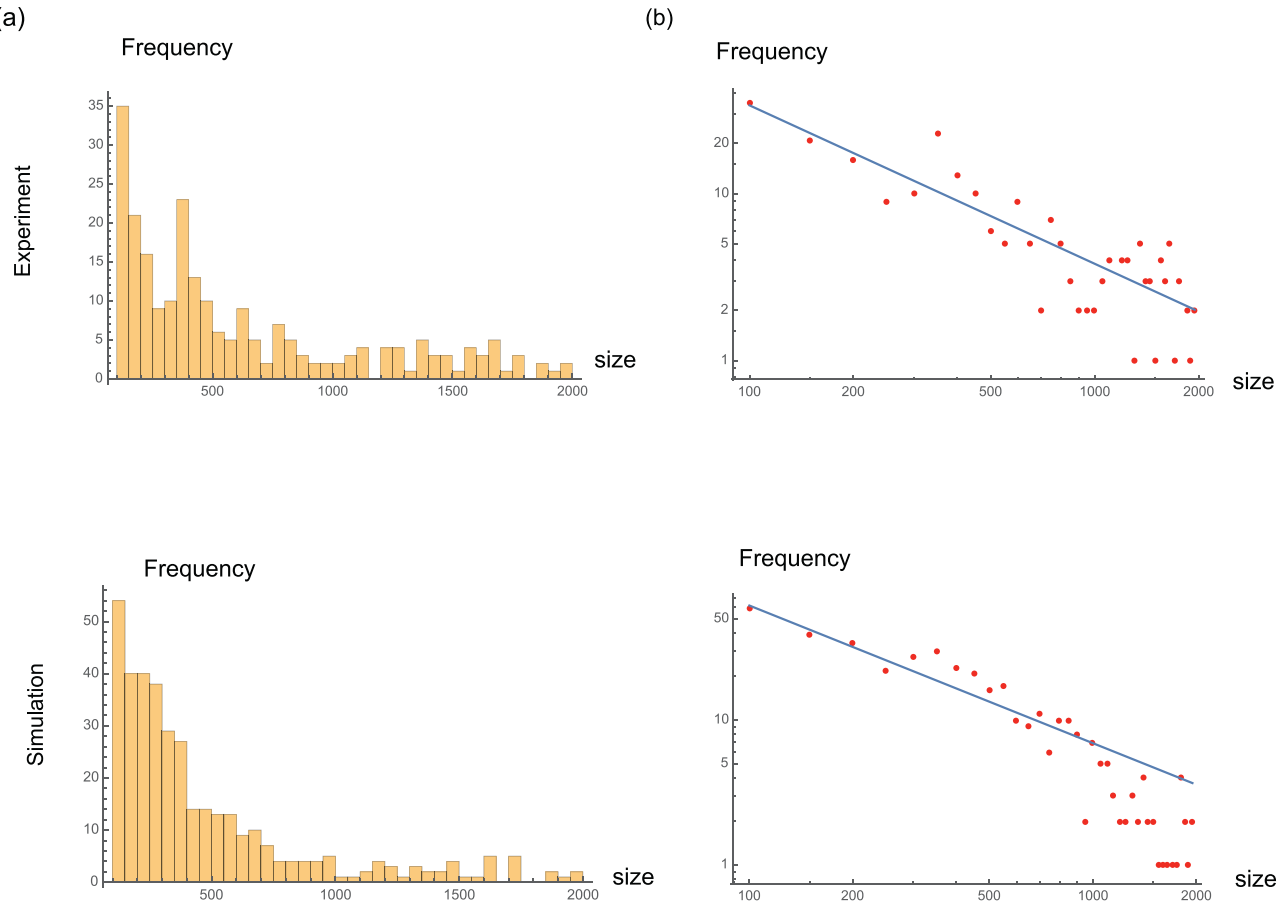

Fig. 6. Size distribution of islands. (a) Histograms of size distribution obtained from experimental and numerical simulation data. (b) Log-log plots of size distributions.

5. Discussion

In our study, we showed that a random searching model reproduced meshwork formation observed in a microdevice, without requiring additional mechanisms. To our knowledge, this is the first report of a mechanism for the intrinsic property of endothelial cells to make perfusable networks in fibrin gels. Previous models, using experiments on Matrigel, attributed mechanics (Manoussaki et al., 1996; van Oers et al., 2014) or chemotaxis (Köhn-Luque et al., 2011; 2013; Merks et al., 2006; Serini et al., 2003) as mechanisms for spontaneous pattern formation. In these models, the system was formulated by partial differential equations and pattern size obtained by deriving the fastest growing wavenumber by linear stability analysis. Although cell shape is known to modify the final pattern in one of these models (Merks et al., 2006), random search by protrusions was not considered. Our results showed that chemotaxis or mechanical deformation of the extracellular matrix were unnecessary to produce a network pattern in this case.

Relationships with percolation theory were considered in our system and a similar analysis was performed in the Matrigel system (Serini et al., 2003). Whether a network percolates is functionally important because it determines whether the endothelial meshwork is perfusable. However, it was still difficult to analytically obtain a percolation threshold in our system. We could obtain a percolation threshold analytically with regular nodes, but our model uses randomly dispersed nodes. In addition, the connection probability function $P(t, l)$ is not simple in our model, making analysis even more difficult.

We tried to obtain a characteristic length of protrusions by dimensional analysis. The characteristic length of protrusions had a dimension of $c/p = 15.3(\mu m)$. The average length of protrusions observed experimentally was $\approx$ 50 μm. Therefore, the characteristic length obtained from dimensional analysis was comparable to the actual characteristic length in the experimental pattern.

The mechanisms by which endothelial cells in fibrin gels extend long protrusions are not clear. Biologically there are two types of cells that are known to extend protrusions, tip cells and mesenchymal cells. In the first hypothesis, the state of cells in fibrin gels was similar to that of the tip cells, specialized cells residing in the tip of the expanding vasculature. The tip cells are known to extend multiple protrusions (Blanco and Gerhardt, 2013). In the second hypothesis, cells extending protrusions have mesenchymal characteristics, having undergone Epithelial–Mesenchimal Transition (EMT). EMT is induced by various growth factors or extracellular matrix components (Lamouille et al., 2014).

Molecules regulating protrusion dynamics may be useful to control meshwork structures. Mechanisms of filopodia formation, elongation and collapse have been well studied (Mattila and Lappalainen, 2008). If protrusions of endothelial cells in fibrin gels are homologous to filopodia, protrusion dynamics could be controlled by modifying the actin cytoskeleton. In this case, cofilin, integrin or mDia2 (Shibue et al., 2013) are potential targets for changing protrusion lengths and numbers. Actin polymerization might also be chemically blocked by cytochalasin D or latrunculin A. The thin and long protrusions may also contain microtubules (Even-Ram et al., 2007; Sagar et al., 2015) because protrusion lengths for endothelial cells in fibrin sometimes exceed 100 μm. Mechanisms controlling microtubules have also been well studied (Conde and Cáceres, 2009). For microtubules, potential target molecules are microtubule associating proteins (MAPs), plus-end tracking pro-

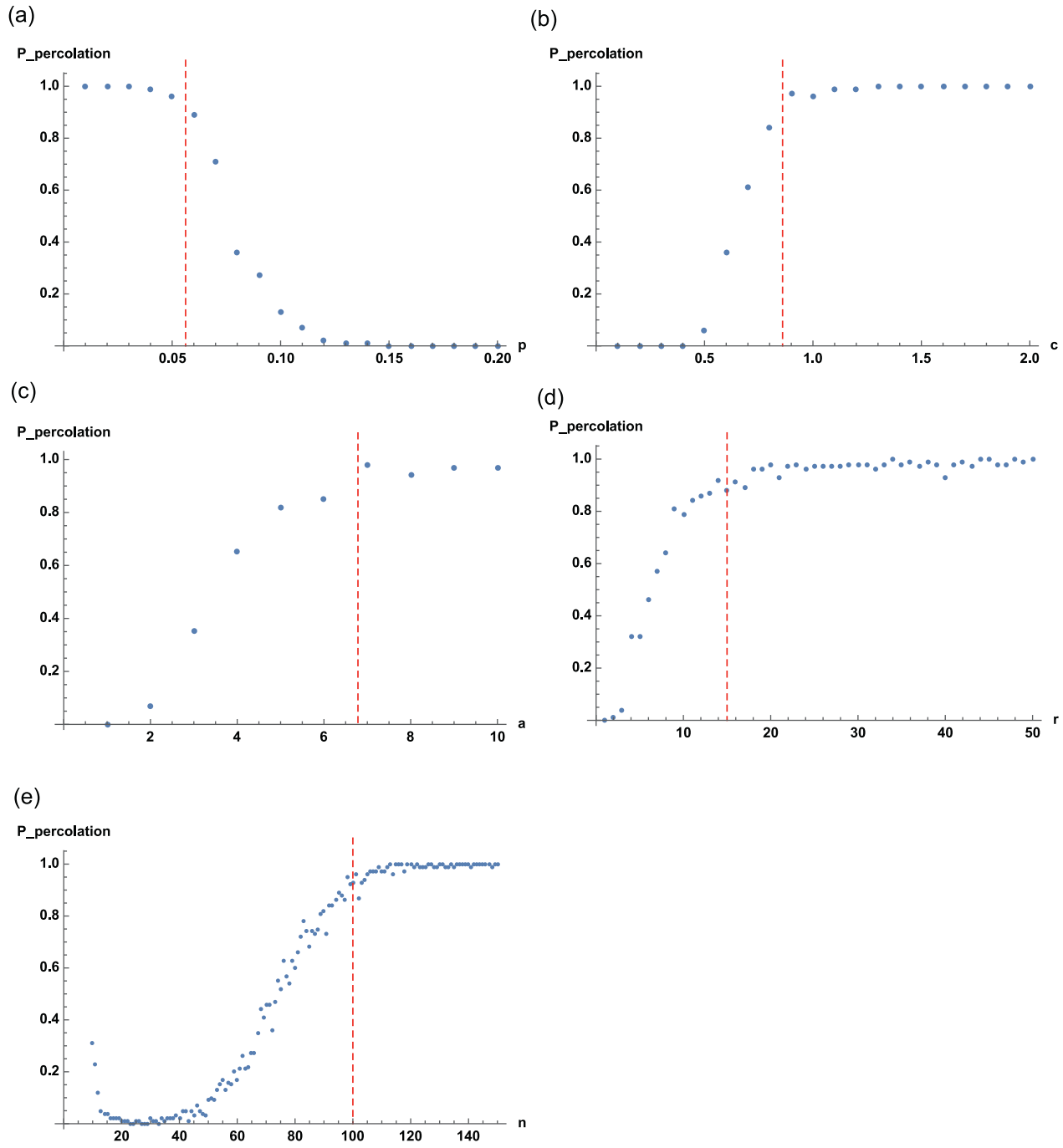

Fig. 7. Effects of parameter changes on percolation threshold. The original value of the parameter is indicated by a dashed line. (a) Collapse probability of a protrusion *p*-percolation probability graph. (b) Protrusion speed *c*-percolation probability graph. (c) Number of protrusions per cell *a*-percolation probability graph. (d) Cell radius *r*-percolation probability graph. (e) Cell number per focal plane *n*-percolation probability graph.

teins (+TIPs), katamin and stathmin. Chemicals available to block microtubule polymerization include colchicine.

Our model of cellular protrusions could be applied to various other processes. The dynamics of this model are similar to those of the cytoskeleton, both involving slower extension and faster collapse of one-dimensional structures (Sagar et al., 2015; Tsygankov et al., 2014). This model can be applied to analyze various processes consisting of constant accumulation and stochastic extinction.

Acknowledgments

The authors would like to thank Shuji Ishihara, Akiko Nakamasu and Yoshiki Kanemitsu for advice on formulating the mathematical model. This work was financially supported by the CREST program of Japan Science and Technology Agency [Grant No. JPMJCR14W4].

Appendix A. Vasculogenesis in fibrin gels

HUVECs were cultivated in EGM-2 medium (Lonza Inc. Basel, Switzerland). Cells were used at passages lower than three for this study. For assays, cells were mixed with 5 mg/ml fibrin gels and

injected in a microdevice (Kim et al., 2013). Human lung fibroblasts were also injected in a different lane of the microdevice to support HUVEC morphogenesis. HUVECs were stained with UEA-1-Alexa 488. Meshwork formation was observed with a Nikon A1 confocal microscope for 12 h (1 frame/5 min). Statistical analysis by the Mann-Whitney *U* test was performed using *Mathematica*.

Appendix B. Particle image velocimetry (PIV)

HUVECs were cultivated in EGM-2 medium and in/on gels on 4-well CELLview cell culture dish (Grainer Bio One International GmbH. Kremsmünster, Austria). Cells were embedded in fibrin gels or seeded on Matrigel. Both gels contained polymer microspheres (Duke Scientific Corp., Palo Alto, California, US), that were mixed with gels to visualize gel deformation. HUVECs were stained with UEA-1-Alexa 488. Meshwork formation was observed with a Nikon A1 confocal microscope for 12 h (1 frame/5 min). Particle Image Velocimetry (PIV) was performed using a PIV plugin for ImageJ (https://sites.google.com/site/qingzongtseng/piv). Supplemental video 1 was obtained by iterative PIV for all time-steps. Means of norm of deformation vectors were 0.17 pixel/frame (in fibrin gels) and 1.73 pixel/frame (on Matrigel). Statistical analysis by the T test was performed using *Mathematica*. The difference was statistically significant ($p = 1.98 \times 10^{-4043}$).

Appendix C. Advection equation representing the protrusion length distribution

Eq. (2) shows the probability distribution of protrusion length. Now we consider the continuous model of protrusive dynamics. These equations represent continuous probability distribution of length:

$$\frac{\partial u}{\partial t} + c\frac{\partial u}{\partial x} = -pu(x,t) \tag{9}$$

$$u(0,t) = \frac{p}{c}\int_{-\infty}^{l} u(x,t)dx \tag{10}$$

$$u(x,0) = \delta(x). \tag{11}$$

(9) states that a protrusion extends at a rate c and collapses with a probability of p per unit time. (10) represents the boundary condition that the length becomes 0 instantaneously if protrusion collapses. (11) describes initial condition. (10) is justified as follows: In the discrete model,

$$Pr(A_{t+\Delta t} = 0) = \sum_{i=-\infty}^{\frac{l}{c\Delta t}-1} Pr(A_t = ic\Delta t) \times p\Delta t. \tag{12}$$

Now $Pr(A_t = x)$ in a discrete model is equivalent to $u(x, t)c\Delta t$ in a continuous model. Therefore, (12) is rewritten as follows:

$$u(0, t+\Delta t) = \sum_{i=-\infty}^{\frac{l}{c\Delta t}-1} u(ic\Delta t, t)c\Delta t \times \frac{p}{c}. \tag{13}$$

Taking the limit of $\Delta t \to 0$,

$$u(0,t) = \frac{p}{c}\int_{-\infty}^{l} u(x,t)dx. \tag{14}$$

Numerical simulations showed that probability distribution by this advection equation was the same as that by the recurrence relation.

We define the connection probability $P_c(t, l)$ as $1 - \int_{-\infty}^{l} u(x,t)dx$. In the discrete model,

$$P(t,l) = 1 - \sum_{i=-\infty}^{\frac{l}{c\Delta t}-1} Pr(A_t = ic\Delta t) \tag{15}$$

$$= 1 - \sum_{i=-\infty}^{\frac{l}{c\Delta t}-1} u(ic\Delta t, t)c\Delta t \tag{16}$$

Taking the limit of $\Delta t \to 0$,

$$P_c(t,l) = 1 - \int_{-\infty}^{l} u(x,t)dx. \tag{17}$$

Considering the probability that a protrusion reaches $x = l$ during $t \sim t + \Delta t$, we obtain the following equation:

$$\begin{aligned} P_c(t+\Delta t, l) - P_c(t,l) &= c\Delta t u(l,t) \\ &= c\Delta t e^{-\frac{lp}{c}} u(0, t - \frac{l}{c}) \\ &= c\Delta t e^{-\frac{lp}{c}} \frac{p}{c}\int_{-\infty}^{l} u(x, t - \frac{l}{c})dx \\ &= pe^{-\frac{lp}{c}}\{1 - P_c(t - \frac{l}{c}, l)\}\Delta t. \end{aligned} \tag{18}$$

By taking limit $\Delta t \to 0$ we obtain following ODE:

$$\frac{dP_c}{dt} = pe^{-\frac{lp}{c}}\{1 - P_c(t - \frac{l}{c}, l)\}. \tag{19}$$

According to (6) and (19), we can obtain the same connection probability from the recurrence relation as from the probability density function. Furthermore, using the analytical solution of $P(t, l)$ (see also Appendix D), we can obtain the analytical solution of $u(x, t)$.

$$\begin{aligned} u(x,t) &= e^{-\frac{px}{c}} u(0, t - \frac{x}{c}) \\ &= e^{-\frac{px}{c}} \frac{p}{c}\int_{-\infty}^{l} u(y, t - \frac{x}{c})dy \\ &= e^{-\frac{px}{c}} \frac{p}{c}\{1 - P(t - \frac{x}{c}, l)\}. \end{aligned} \tag{20}$$

Appendix D. Derivation of the analytical solution

D1. The analytical solution can be calculated recursively.

In this subsection, we show that the delay differential Eq. (6) is solved in a stepwise fashion.

For simplicity, we define $\alpha = pe^{-\frac{lp}{c}}$, $\beta = \frac{l}{c}$.

(i) When $0 \le t < \beta$,

$$P(t,l)|_{0\le t<\beta} = 0. \tag{21}$$

(ii) When $\beta \le t \le 2\beta$,

$$\frac{dP}{dt} = \alpha\{1 - 0\} = \alpha \tag{22}$$

$$P(\beta, l) = \frac{\alpha}{p}. \tag{23}$$

From (22) and (23) we obtain

$$P(t,l)|_{\beta\le t\le 2\beta} = -\alpha\beta + \frac{\alpha}{p} + \alpha t. \tag{24}$$

(iii) When $2\beta \le t \le 3\beta$,

$$\begin{aligned} P(t,l)|_{2\beta\le t\le 3\beta} = &-2\alpha^2\beta^2 - \alpha\beta + \frac{2\alpha^2\beta}{p} + \frac{\alpha}{p} - \frac{\alpha^2 t}{p} - \frac{1}{2}\alpha^2 t^2 \\ &+2\alpha^2\beta t + \alpha t. \end{aligned} \tag{25}$$

(iv) When $3\beta \le t \le 4\beta$,

$$P(t,l)|_{3\beta\le t\le 4\beta} = -\frac{9\alpha^3\beta^3}{2} - 2\alpha^2\beta^2 - \alpha\beta + \frac{9\alpha^3\beta^2}{2p} + \frac{2\alpha^2\beta}{p} + \frac{\alpha}{p} + \frac{\alpha^3t^2}{2p} - \frac{3\alpha^3\beta t}{p} - \frac{\alpha^2 t}{p} + \frac{\alpha^3t^3}{6} - \frac{3}{2}\alpha^3\beta t^2 - \frac{\alpha^2t^2}{2} + \frac{9}{2}\alpha^3\beta^2 t + 2\alpha^2\beta t + \alpha t. \quad (26)$$

$P(t,l)|_{n\beta\le t\le(n+1)\beta}$ can be obtained by repeating this procedure.

D2. Differences between functions show certain regularity.

Now we define $Q_n(t)$ as follows:

$$Q_n(t) = P(t,l)|_{n\beta\le t\le(n+1)\beta} - P(t,l)|_{(n-1)\beta\le t\le n\beta}. \quad (27)$$

Then

$$Q_1(t) = \alpha\left(-\beta + \frac{1}{p} + t\right)$$

$$Q_2(t) = -\frac{\alpha^2(t-2\beta)(pt-2\beta p+2)}{2p}$$

$$Q_3(t) = \frac{\alpha^3(t-3\beta)^2(pt-3\beta p+3)}{6p}.$$

From this relation, we expect $Q_n(t)$ as follows:

$$Q_n(t) = \frac{(-1)^{n-1}\alpha^n(t-n\beta)^{n-1}(pt-n\beta p+n)}{n!\,p}. \quad (28)$$

If (28) holds, we solve the delay differential Eq. (6).

$$P(t,l)|_{n\beta\le t\le(n+1)\beta} = \sum_{k=1}^{n} Q_k(t) \equiv R_n(t). \quad (29)$$

D3. Derivation of the analytical solution by mathematical induction for (29).

(i) For $n=1$, (29) holds since $R_1(t) = Q_1(t)$.
(ii) Suppose (29) is true for some $n = j \ge 1$. Then

$$R_j(t) = \sum_{k=1}^{j} Q_k(t). \quad (30)$$

When $n = j+1$, we have

$$R'_{j+1}(t) = -\alpha R_j(t-\beta) + \alpha \quad (31)$$

$$R_{j+1}(t) = -\alpha\sum_{k=1}^{j}\{\int Q_k(t-\beta)dt\} + \alpha\int dt = \sum_{k=1}^{j} Q_{k+1}(t) + \alpha t + C_j \quad (32)$$

where C_j is a constant of integration. R is continuous at $t = (j+1)\beta$,

$$R_{j+1}((j+1)\beta) = R_j((j+1)\beta)$$

$$C_j = \frac{\alpha}{p} - \alpha\beta. \quad (33)$$

Therefore,

$$R_{j+1}(t) = \sum_{k=1}^{j} Q_{k+1}(t) + \alpha t + \frac{\alpha}{p} - \alpha\beta = \sum_{k=2}^{j+1} Q_k(t) + Q_1(t) = \sum_{k=1}^{j+1} Q_k(t). \quad (34)$$

Consequently, (29) holds for arbitrary positive integer n.

Appendix E. Parameter fitting

Experimental period t, elongation speed c and mean cell radius r were already known from the experimental data. We also obtained the relationship between distance l and connection probability $P(t, l)$. Mean protrusion number a and collapse probability per unit time p are difficult to obtain from experimental data. To obtain a and p, we substituted t, c and r by experimentally obtained values. Then $P(t, l)$ were fitted to the experimentally obtained distance-connection probability relation by the least squares method. The obtained values are considered as reasonable because they reproduce meshwork morphology effectively.

Appendix F. Derivation of conditional probability of connection to express the time course of meshwork formation

We define $Pr(t) = P(t,l), Pr(\bar{t}) = 1 - P(t,l)$. Considering the conditional probability $Pr(t_2|\bar{t_1})$ $(t_2 > t_1)$, we obtain the connection probability from time t_1 to t_2.

$$Pr(t_2|\bar{t_1}) = \frac{Pr(\bar{t_1}\cap t_2)}{Pr(\bar{t_1})} = \frac{1 - Pr(t_1\cap t_2) - Pr(t_1\cap\bar{t_2}) - Pr(\bar{t_1}\cap\bar{t_2})}{1 - Pr(t_1)} = \frac{1 - Pr(t_1) - 0 - (1 - Pr(t_2))}{1 - Pr(t_1)} = \frac{Pr(t_2) - Pr(t_1)}{1 - Pr(t_1)} \quad (35)$$

Therefore, conditional probability can be obtained from $P(t, l)$.

Supplementary material

Supplementary material associated with this article can be found, in the online version, at doi:10.1016/j.jtbi.2017.06.012.

References

Adams, R.H., Alitalo, K., 2007. Molecular regulation of angiogenesis and lymphangiogenesis. Nat. Rev. Mol. Cell Biol. 8 (6), 464–478. doi:10.1038/nrm2183.

Blanco, R., Gerhardt, H., 2013. VEGF and notch in tip and stalk cell selection. Cold Spring Harb. Perspect. Med. 3 (1), a006569. doi:10.1101/cshperspect.a006569.

Conde, C., Cáceres, A., 2009. Microtubule assembly, organization and dynamics in axons and dendrites. Nat. Rev. Neurosci. 10 (5), 319–332. doi:10.1038/nrn2631.

Drake, C.J., 2003. Embryonic and adult vasculogenesis. Birth Defects Res. C: Embryo Today: Rev. 69 (1), 73–82. doi:10.1002/bdrc.10003.

Even-Ram, S., Doyle, A.D., Conti, M.A., Matsumoto, K., Adelstein, R.S., Yamada, K.M., 2007. Myosin IIA regulates cell motility and actomyosinmicrotubule crosstalk. Nat. Cell Biol. 9 (3), 299–309. doi:10.1038/ncb1540.

Gamba, A., Ambrosi, D., Coniglio, A., de Candia, A., Di Talia, S., Giraudo, E., Serini, G., Preziosi, L., Bussolino, F., 2003. Percolation, morphogenesis, and burgers dynamics in blood vessels formation. Phys. Rev. Lett. 90 (11), 118101. doi:10.1103/PhysRevLett.90.118101.

Gilbert, S.F., 2014. Developmental Biology, 10th Sinauer, Andrew D.

Hasan, A., Paul, A., Vrana, N.E., Zhao, X., Memic, A., Hwang, Y.-S., Dokmeci, M.R., Khademhosseini, A., 2014. Microfluidic techniques for development of 3D vascularized tissue. Biomaterials 35 (26), 7308–7325. doi:10.1016/j.biomaterials.2014.04.091.

Kim, S., Lee, H., Chung, M., Jeon, N.L., 2013. Engineering of functional, perfusable 3D microvascular networks on a chip. Lab Chip 13 (8), 1489–1500. doi:10.1039/c3lc41320a.

Köhn-Luque, A., de Back, W., Starruß, J., Mattiotti, A., Deutsch, A., Pérez-Pomares, J.M., Herrero, M.A., 2011. Early embryonic vascular patterning by matrix-mediated paracrine signalling: a mathematical model study. PLoS One 6 (9), e24175. doi:10.1371/journal.pone.0024175.

Köhn-Luque, A., de Back, W., Yamaguchi, Y., Yoshimura, K., Herrero, M.A., Miura, T., 2013. Dynamics of VEGF matrix-retention in vascular network patterning. Phys. Biol. 10 (6), 066007. doi:10.1088/1478-3975/10/6/066007.

Kubota, Y., Kleinman, H.K., Martin, G.R., Lawley, T.J., 1988. Role of laminin and basement membrane in the morphological differentiation of human endothelial cells into capillary-like structures. J. Cell Biol. 107 (4), 1589–1598.

Lamouille, S., Xu, J., Derynck, R., 2014. Molecular mechanisms of epithelialmesenchymal transition. Nat. Rev. Mol. Cell Biol. 15 (3), 178–196. doi:10.1038/nrm3758.

Manoussaki, D., Lubkin, S.R., Vernon, R.B., Murray, J.D., 1996. A mechanical model for the formation of vascular networks in vitro. Acta Biotheor. 44 (3–4), 271–282.

Mattila, P.K., Lappalainen, P., 2008. Filopodia: molecular architecture and cellular functions. Nat. Rev. Mol. Cell Biol. 9 (6), 446–454. doi:10.1038/nrm2406.

Merks, R.M., Brodsky, S.V., Goligorksy, M.S., Newman, S.A., Glazier, J.A., 2006. Cell elongation is key to in silico replication of in vitro vasculogenesis and subsequent remodeling. Dev. Biol. 289 (1), 44–54. doi:10.1016/j.ydbio.2005.10.003.

Miura, T., Tanaka, R., 2009. In vitro vasculogenesis models revisited - measurement of VEGF diffusion in matrigel. Math. Model Nat. Phenom. 4 (4), 118–130. doi:10.1051/mmnp/20094404.

Miura, T., Yokokawa, R., 2016. Tissue culture on a chip: developmental biology applications of self-organized capillary networks in microfluidic devices. Dev. Growth Differ. 58 (6), 505–515. doi:10.1111/dgd.12292.

van Oers, R.F.M., Rens, E.G., LaValley, D.J., Reinhart-King, C.A., Merks, R.M.H., 2014. Mechanical cell-matrix feedback explains pairwise and collective endothelial cell behavior in vitro. PLoS Comput. Biol. 10 (8), e1003774. doi:10.1371/journal.pcbi.1003774.

Sagar, Pröls, F., Wiegreffe, C., Scaal, M., 2015. Communication between distant epithelial cells by filopodia-like protrusions during embryonic development. Development 142 (4).

Serini, G., Ambrosi, D., Giraudo, E., Gamba, A., Preziosi, L., Bussolino, F., 2003. Modeling the early stages of vascular network assembly. EMBO J. 22 (8), 1771–1779. doi:10.1093/emboj/cdg176.

Shibue, T., Brooks, M.W., Weinberg, R.A., 2013. An integrin-linked machinery of cytoskeletal regulation that enables experimental tumor initiation and metastatic colonization. Cancer Cell 24 (4), 481–498. doi:10.1016/j.ccr.2013.08.012.

Tsygankov, D., Bilancia, C.G., Vitriol, E.A., Hahn, K.M., Peifer, M., Elston, T.C., 2014. Cellgeo: a computational platform for the analysis of shape changes in cells with complex geometries. J. Cell Biol. 204 (3).